



# One-step synthesis of CdS nanoparticles/MoS<sub>2</sub> nanosheets heterostructure on porous molybdenum sheet for enhanced photocatalytic H<sub>2</sub> evolution

Lili Zhao <sup>a,b</sup>, Jin Jia <sup>b</sup>, Zhiyuan Yang <sup>a</sup>, Jiayuan Yu <sup>b</sup>, Aili Wang <sup>b</sup>, Yuanhua Sang <sup>a,\*</sup>, Weijia Zhou <sup>b,\*</sup>, Hong Liu <sup>a,\*</sup>

<sup>a</sup> State Key Laboratory of Crystal Materials, Shandong University, 27 Shandan Road, Jinan, Shandong, 250100, China

<sup>b</sup> School of Environment and Energy, Guangdong Provincial Key Laboratory of Atmospheric Environment and Pollution Control, South China University of Technology, Guangzhou Higher Education Mega Center, Guangzhou, Guangdong, 510006, China

## ARTICLE INFO

### Article history:

Received 13 February 2017

Received in revised form 28 March 2017

Accepted 1 April 2017

Available online 2 April 2017

### Keywords:

Co-catalysts

Non-noble metal

Conductive supports

Photocatalytic H<sub>2</sub> evolution

Porous

## ABSTRACT

Co-catalysts for H<sub>2</sub> production are often made from expensive noble metals, such as the most efficient Pt. The alternative non-noble metal co-catalysts with low cost and high efficiency are therefore highly desirable for economically viable H<sub>2</sub> production. Herein, we demonstrated that a CdS/MoS<sub>2</sub>/Mo sheets system simultaneously containing photocatalysts, co-catalysts, and conductive supports, was prepared via the one-step hydrothermal process by Mo sheets as template and Mo sources. The obtained CdS/MoS<sub>2</sub>/Mo sheets possess the superior photocatalytic H<sub>2</sub> production via water splitting under visible light irradiation, which achieved an extraordinary H<sub>2</sub> production of 4540  $\mu\text{mol h}^{-1} \text{g}^{-1}$ , up to 28.6 and 3.6 times greater than that of CdS alone and Pt/CdS. The synergistic effect of MoS<sub>2</sub> as co-catalysts and Mo sheets as conductive supports contribute to the dramatically improved photocatalytic H<sub>2</sub> evolution activity of CdS photocatalysts, by means of facilitating charge carriers separation and providing active sites for proton reduction. These findings provide a straightforward and practical route to produce cheap and efficient co-catalysts for large-scale water splitting.

© 2017 Elsevier B.V. All rights reserved.

## 1. Introduction

With the increasing global energy demand and the environmental pollution from fossil fuels, hydrogen as a clean and renewable power source attracts more attentions. Steam methane reforming [1] and the water–gas shift reaction [2] are currently major H<sub>2</sub> production approaches in industry. However, this energy conversion process will release large amounts of CO<sub>2</sub> to the ambient environment. The conversion of solar energy into hydrogen fuels by photocatalytic water splitting using semiconductors as catalysts is considered as one of the most promising ways to solve the energy crisis [3–6] and offers the potential of H<sub>2</sub> supply with a low to zero carbon footprint [7]. Since the first report on water splitting from Fujishima and Honda in 1972 [8], numerous studies on the semiconductor materials for photocatalytic hydrogen evolution reaction (HER) have been developed, such as TiO<sub>2</sub> [9–12], ZnO [13], C<sub>3</sub>N<sub>4</sub> [14]

and CdS [15–17]. Among these, cadmium sulfide (CdS) is of considerable interest due to its appropriate band gap (2.42 eV) for efficient absorption of visible light and its suitable conduction band for HER. Numerous studies on photocatalytic water splitting by using CdS as photocatalyst have been made [15,18,19]. But the extremely low activity for photocatalytic hydrogen production due to the rapid photogenerated electron–holes recombination, lack of active sites for proton reduction and photo-corrosion remain significant challenges for HER.

To further improve the performance of CdS for photocatalytic hydrogen production, various strategies have been adopted [15,20–22]. Loading co-catalysts onto CdS and loading CdS onto conductive supports are regarded as the effective strategies for improving photocatalytic H<sub>2</sub> production. In general, the loading co-catalysts on semiconductor photocatalysts not only provides the HER active sites, but also is an effective way to inhibit the charge carrier recombination of photocatalysts. It is well known that the loading of Pt as a co-catalyst on photocatalysts significantly enhances the photocatalytic H<sub>2</sub> production efficiency [23]. However, Pt is a rare and expensive noble metal, which limits the widespread application in photocatalytic H<sub>2</sub> production. There-

\* Corresponding authors.

E-mail addresses: [sangyh@sdu.edu.cn](mailto:sangyh@sdu.edu.cn) (Y. Sang), [eszhouwj@scut.edu.cn](mailto:eszhouwj@scut.edu.cn) (W. Zhou), [hongliu@sdu.edu.cn](mailto:hongliu@sdu.edu.cn) (H. Liu).

fore, alternative co-catalysts based on non-noble metal materials have been actively pursued. Currently, transition metal dichalcogenides (TMDs) [24,25] with the layered structures, especially  $\text{MoS}_2$ , has been demonstrated to be highly efficient co-catalyst in photocatalytic  $\text{H}_2$  production. Li's group first reported  $\text{MoS}_2$  loaded on  $\text{CdS}$  by a chemical method for photocatalytic  $\text{H}_2$  production [15], the significant enhancement of the photocatalytic  $\text{H}_2$  production activity even exceeds the photocatalytic activities of Pt and other noble metals loaded on  $\text{CdS}$ . Besides, the presence of conductive supports, such as graphene nanosheets and metal supports, can facilitate the separation of photoinduced electron-hole pairs, since photogenerated electrons can migrate through the conductive supports. Zhang's group prepared  $\text{CdS}$  nanoparticles/ $\text{Cd}$  nanosheets heterostructures, which exhibit superior photocatalytic  $\text{H}_2$  production activity under visible light illumination compared to unsupported  $\text{CdS}$  nanoparticles and supported onto carbon nanotubes or reduced graphene oxide. The enhancement in  $\text{H}_2$  production can be attributed to the superior electrical conductivity of  $\text{Cd}$  nanosheets [26].

Herein, we report a heterostructure of  $\text{CdS}/\text{MoS}_2$  nanosheets derived from Mo sheets, which is synthesized via a one-step hydrothermal process by Mo sheets as template and Mo sources. The obtained  $\text{CdS}/\text{MoS}_2/\text{Mo}$  sheets simultaneously contain co-catalysts of  $\text{MoS}_2$  nanosheets, photocatalysts of  $\text{CdS}$  and conductive supports of Mo sheets for photocatalytic  $\text{H}_2$  production. Mo sheets as conductive bridges facilitate the migration of photo-generated electron between  $\text{CdS}$  and  $\text{MoS}_2$ . Compared to the  $\text{CdS}$  and  $\text{CdS}/\text{MoS}_2$ , the  $\text{CdS}/\text{MoS}_2/\text{Mo}$  sheets possess the significantly enhanced photocatalytic HER activity with an excellent  $\text{H}_2$  production of  $4540 \mu\text{mol h}^{-1} \text{g}^{-1}$  and robust catalytic stability.

## 2. Experimental section

### 2.1. Chemicals

The analytical pure (AR) of molybdenum trioxide ( $\text{MoO}_3$ ), cadmium acetate ( $\text{Cd}(\text{CH}_3\text{COO})_2 \cdot 2\text{H}_2\text{O}$ ) and thioacetamide ( $\text{CH}_3\text{CSNH}_2$ ) were purchased from Sinopharm Chemical Reagents Beijing Co. Deionized water was supplied with a Barnstead Nanopure Water System ( $18.3 \text{ M}\Omega\text{-cm}$ ) and was used throughout this experiment.

### 2.2. Synthesis of Mo sheets and $\text{CdS}/\text{MoS}_2/\text{Mo}$ sheets hybrid catalysts

The Mo sheets were prepared from  $\text{MoO}_3$  precursors through temperature programmed reduction in the flowing  $\text{Ar-H}_2$  (10%) mixture gas. The  $\text{MoO}_3$  powders were quickly heated from room temperature to  $900^\circ\text{C}$  with a heating rate of  $20^\circ\text{C}/\text{min}$  and were maintained at  $900^\circ\text{C}$  for 4 h under an  $\text{Ar-H}_2$  (10%) mixture gas flow. Finally, the gray Mo sheets were collected from the quartz tube wall at the hot center of the tube furnace. The  $\text{CdS}/\text{MoS}_2/\text{Mo}$  sheets hybrid catalysts were prepared via a simple hydrothermal method by using the above prepared Mo sheets as template and Mo sources. Specifically, 5.0 mmol cadmium acetate and some amount of thioacetamide were dissolved in 40 mL of deionized water and stirred for 15 min, then a certain amount of as-obtained Mo sheets were added by vigorous stirring and ultrasonic treatment to obtain a uniformly dispersed suspension. In order to control the different  $\text{MoS}_2$  loading amounts of  $\text{CdS}/\text{MoS}_2/\text{Mo}$  sheets hybrid catalysts for comparison, the molar ratio of  $\text{Mo/Cd} = 5/1, 2/1, 1/1, 1/2, 1/5$  was used. Then the suspension was transferred to a 50 mL Teflon-lined stainless steel autoclave and maintained at  $200^\circ\text{C}$  for 24 h. The resulted powders were washed with deionized water and ethanol several times and dried at  $60^\circ\text{C}$  for 24 h. Pure  $\text{CdS}$  and  $\text{CdS}/\text{MoS}_2$

were prepared without the addition of Mo sheets or using  $\text{MoO}_3$  instead of Mo sheet, respectively. For comparison, loading 2 wt% Pt on  $\text{CdS}$  nanoparticles was prepared by a photoreduction process. Namely, a certain amount of  $\text{H}_2\text{PtCl}_6$  ( $10 \text{ mg mL}^{-1}$ ) in methanol aqueous solution (20 mL methanol and 80 mL water) was firstly prepared, after  $\text{CdS}$  nanoparticles were added, it was irradiated with a Xe arc lamp (300 W) for 1 h.

### 2.3. Characterization

The morphologies, structure, and thickness of the samples were detected by a field emission scanning electron microscope (FESEM, MERLIN Compact, Carl Zeiss), high-resolution transmission electron microscopy (HRTEM, JEM-2100F, at an acceleration voltage of 200 kV) and atomic force microscope (AFM, Bruker Multimode 8). Brunauer-Emmet-Teller (BET) surface area was analyzed by using a Quantachrome Autosorb-iQ2 instrument with nitrogen adsorption at  $77 \text{ K}$  using the Barrett-Joyner-Halenda (BJH) method. The crystal structure and elementary composition were performed on a D8 Advance (Germany Bruker) X-ray diffractometer (XRD) with  $\text{Cu K}\alpha$  radiation ( $\lambda = 0.15406 \text{ nm}$ ) and X-ray photoelectron spectra (XPS, Ulvac-Phi) measurement. The UV-vis absorption spectra of samples were recorded by a UV-vis spectrophotometer (UV-6100, Metash). The different loading amounts of  $\text{MoS}_2$  for  $\text{CdS}/\text{MoS}_2/\text{Mo}$  sheets system were calculated by measuring the sulfur element content in  $\text{MoS}_2/\text{Mo}$  sheets on a QL-HW2000 B high-frequency infrared ray carbon/sulfur analyzer. Typically, according to the sulfur element content in  $\text{MoS}_2/\text{Mo}$  sheets (4.40 wt%), the molar percentage of  $\text{MoS}_2$  from sulfuration of Mo sheet can be calculated to be 6.9 mol%. Assuming that the cadmium acetate was completely transferred into  $\text{CdS}$ , and combine the molar ratio of  $\text{Mo/Cd} = 5/1, 2/1, 1/1, 1/2, 1/5$ , the different amount of loading  $\text{MoS}_2$  can be calculated. Take  $\text{Mo/Cd} = 5/1$  as example, the mass amount of loading  $\text{MoS}_2$  can be calculated from the following equation:

$$\text{mass amount of MoS}_2 \text{ (wt\%)} = \frac{160.07 \times (5 \times 6.9 \text{ mol\%})}{95.94 \times (5 - 5 \times 6.9 \text{ mol\%}) + 160.07 \times (5 \times 6.9 \text{ mol\%}) + 144.46 \times 1}$$

### 2.4. Photocatalytic hydrogen evolution

The photocatalytic hydrogen evolution experiments were performed in a closed quartz round-bottom flask. During the photocatalysis, a 300 W xenon arc lamp equipped with a 420 nm cut-off filter was used as the light sources, which was positioned 10 cm away from the reactor and giving an irradiation of  $52.2 \text{ mW cm}^{-2}$ . Typically, 10 mg of the as-obtained  $\text{CdS}/\text{MoS}_2/\text{Mo}$  sheets hybrid catalysts was dispersed in a mixed aqueous solution containing 0.35 M  $\text{Na}_2\text{S}$  and 0.25 M  $\text{Na}_2\text{SO}_3$ . Before irradiation, the system was bubbled with nitrogen for 30 min to remove the air. The produced hydrogen was analyzed by an online gas chromatograph equipped with a thermal conductivity detector (HXSP-GC950, China, TCD, nitrogen as a carrier gas and 5 Å molecular sieve column).

The apparent quantum efficiency (QE) defined by the following equation were measured using a 300 W xenon arc lamp equipped with a 420 nm cut-off filter and an irradiatometer:

$$\text{QE (\%)} = \frac{\text{number of reacted electrons}}{\text{number of incident photons}} \times 100\% = \frac{\text{number of evolved H}_2 \text{ molecules} \times 2}{\text{number of incident photons}}$$

The power of the light was  $0.080 \text{ J s}^{-1}$ , corresponding to the number of incident photons ( $1.811 \times 10^{17}$  photons per s),

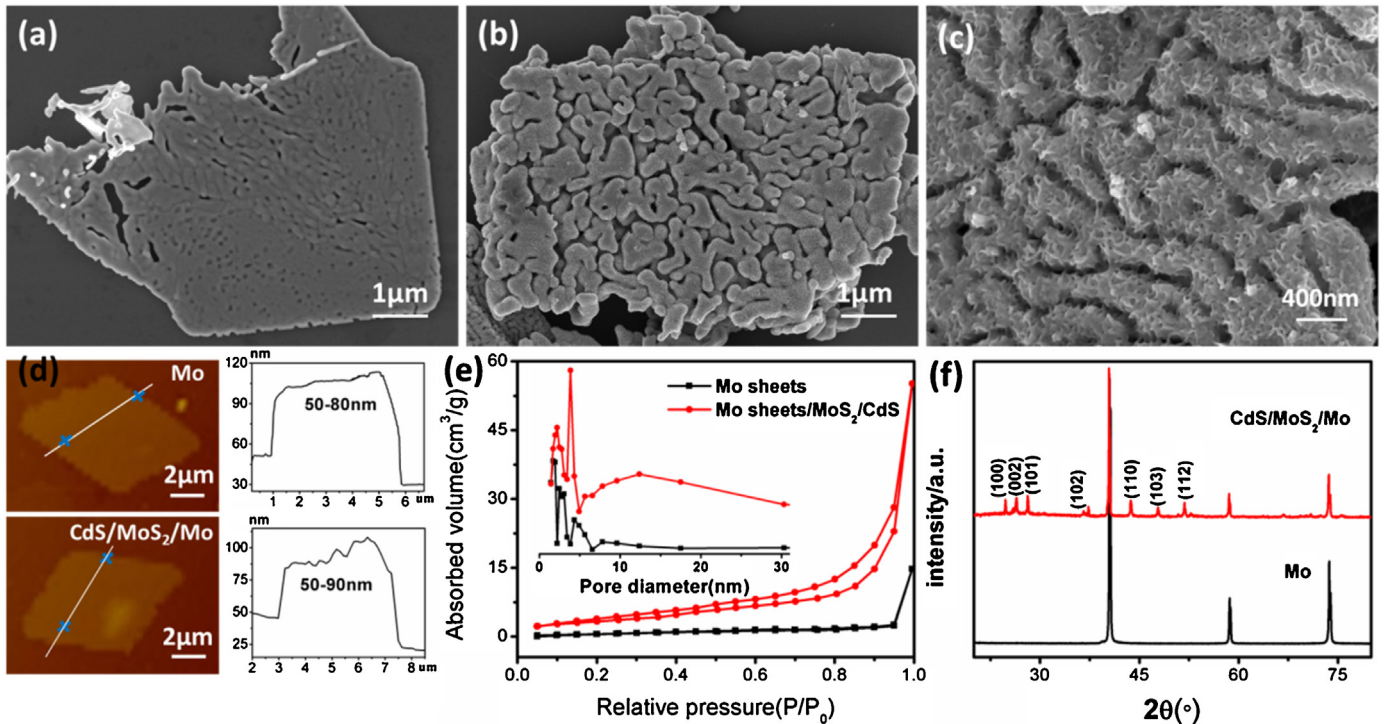


**Fig. 1.** SEM images of (a) Mo sheets, (b,c) CdS/MoS<sub>2</sub>/Mo sheets, AFM images (d) and N<sub>2</sub> adsorption–desorption isotherms (e) and XRD patterns (f) of Mo sheets and CdS/MoS<sub>2</sub>/Mo sheets. Inset of Fig. 1e is the corresponding pore size distribution of Mo sheets and CdS/MoS<sub>2</sub>/Mo sheets.

which was measured using an irradiatometer (CEL-NP2000, Beijing CEAULIGHT Technology co., LTD).

### 2.5. Photoelectrochemical measurements

Photoelectrochemical (PEC) analysis was performed on an electrochemical workstation (CHI 760C, CH Instruments Inc.) in 0.5 M H<sub>2</sub>SO<sub>4</sub> aqueous solution with a three-electrode configuration. In the PEC, CdS/MoS<sub>2</sub>/Mo sheets hybrid catalysts modified on glassy carbon electrode, a carbon rod and Hg/Hg<sub>2</sub>Cl<sub>2</sub> electrode (SCE, saturated KCl) were used as the working electrode, counter and reference electrodes, respectively. The working electrodes were prepared as follows: 5 mg of the hybrid catalyst powders was dispersed in 1 mL of 1:1 (v: v) water/ethanol mixed solvents along with 25  $\mu$ L of Nafion solution (~10% in a mixture of alcohols and water). After the mixture was sonicated for 30 min, 5  $\mu$ L of the above suspension was drop-cast onto the glassy carbon electrode with a geometrical surface area of 0.07 cm<sup>2</sup>. With the light irradiation by a 300 W xenon lamp, polarization curves in the dark and light were recorded by in the sweep range from 0 to  $-0.5$  V vs. RHE at a potential sweep rate of 5 mV/s. The photocurrent response (i–t) curves were recorded at  $-0.1$  V vs. RHE for all the samples. Electrochemical impedance spectroscopy (EIS) was carried out with an amplitude of 10 mV and a frequency range from 100 kHz to 0.01 Hz.

## 3. Results and discussion

The morphology and structure of Mo sheets and CdS/MoS<sub>2</sub>/Mo sheets were characterized by SEM, AFM, BET, and XRD, as shown in Fig. 1. From Fig. 1a, the morphology of as-obtained Mo is a sheet-like shape with an irregular edge around 4–6  $\mu$ m and a thickness of dozens of nanometers. The average thickness of Mo sheets was determined by AFM for 50–80 nm in Fig. 1d. Also, it can be observed that the surface of Mo sheets is smooth and there are only a few small pores (Fig. 1a). After the reaction with cadmium acetate and sulfurization, the surface of as-obtained CdS/MoS<sub>2</sub>/Mo

sample becomes rough, and a large number of worm-like pores occur (Fig. 1b), which also remains the sheet morphology. The thin MoS<sub>2</sub> nanosheets uniformly coated on the surface of Mo sheets can be clearly seen in Fig. 1c. No distinct CdS photocatalysts were observed, this may be due to the small size and perfect combination with MoS<sub>2</sub> nanosheets. The average thickness of obtained CdS/MoS<sub>2</sub>/Mo sheets was slightly increased due to the loading of MoS<sub>2</sub>/CdS, which was around 50–90 nm confirmed by AFM (Fig. 1d). The AFM image with the rugged altitude line also confirmed the rough and worm-like porous surface of CdS/MoS<sub>2</sub>/Mo sheets. N<sub>2</sub> adsorption–desorption isotherms (Fig. 1e) of the CdS/MoS<sub>2</sub>/Mo sheets confirmed the porous structure with a specific surface area of 23.669 m<sup>2</sup> g<sup>-1</sup>, which was much larger than that of Mo sheets (7.097 m<sup>2</sup> g<sup>-1</sup>). The corresponding pore size distribution of 2 nm–5 nm was observed for both Mo sheets and CdS/MoS<sub>2</sub>/Mo sheets. However, after the sulfurization, the broad size distribution of 5 nm–30 nm was detected in CdS/MoS<sub>2</sub>/Mo sheets, implying that the sulfurization process expands the pore structure of sheets, which was also observed by SEM images. The XRD pattern (Fig. 1f) shows the perfect crystallization of metallic Mo with characteristic peaks ( $2\theta$ ) at 40.5°, 58.6°, and 73.7° (JCPDS card 42-1120). After the reaction with cadmium and sulfurization, the intensity of diffraction peaks of Mo decreases, but remains the main diffraction peaks, implying the existence of Mo sheet as the substrate. Some new strong peaks at 24.8°, 26.5°, 28.2°, 36.6°, 43.7°, 47.9° and 51.9° were attributed to (100) (002) (101) (102) (110) (103) and (112) planes of CdS (JCPDS card 77-2306), respectively. The diffraction peaks of MoS<sub>2</sub> were not observed due to its weaker crystallization compared with metallic Mo and CdS.

The morphology and structure of obtained CdS/MoS<sub>2</sub>/Mo sheets were also studied by (HR)TEM, as well as energy dispersive X-ray spectrometry (EDS) mapping, as shown in Fig. 2. The TEM image of CdS/MoS<sub>2</sub>/Mo sheets in Fig. 2a is in good agreement with the worm-like porous structure in the SEM image (Fig. 1b). Due to the existence of Mo sheets as a core, the electrons were hard to penetrate through CdS/MoS<sub>2</sub>/Mo sheets, causing the TEM image

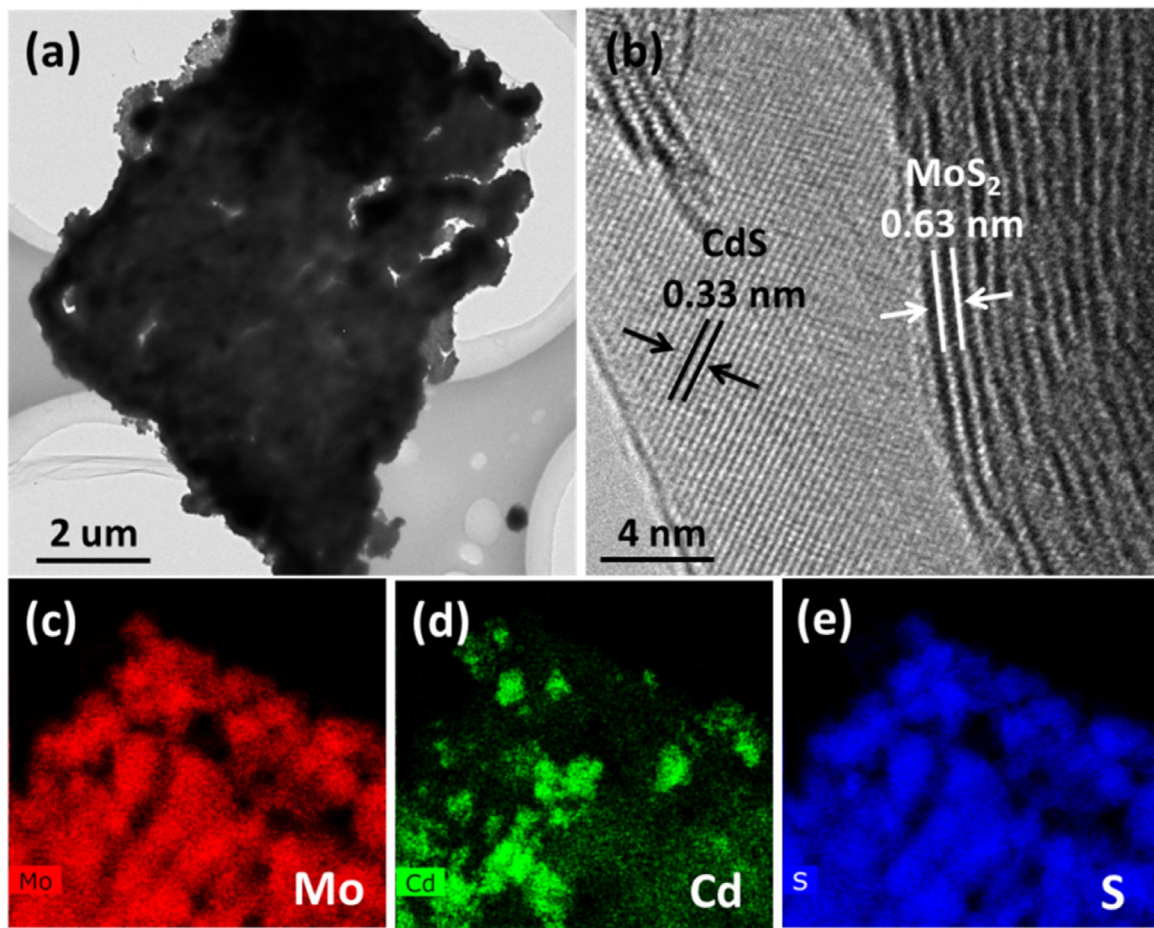


**Fig. 2.** The nanostructure of the as-obtained CdS/MoS<sub>2</sub>/Mo sheets: (a) Transmission electron microscopy (TEM), (b) HRTEM images and (c–e) EDS element mapping for Mo, Cd and S equipped on TEM.

with deep contrast. The magnified HRTEM image in Fig. 2b displays two kinds of lattice spacing. The fringe with the lattice spacing of approximately 0.63 nm corresponds to the (002) plane of layered MoS<sub>2</sub> [27], and the other fringe with a lattice spacing of approximately 0.33 nm is ascribed to the (111) plane of cubic CdS [28]. These results indicate that MoS<sub>2</sub> and CdS have been successfully synthesized on the surface of Mo sheets, the effective interface between CdS and MoS<sub>2</sub> is beneficial to the electronic transmission. The elemental analysis with EDS mapping (Fig. 2c–e) confirms the uniform distribution of Mo, Cd and S in the CdS/MoS<sub>2</sub>/Mo sheets, confirming the formation of a perfect combination between MoS<sub>2</sub> nanosheets and CdS photocatalyst.

To further investigate the surface chemical composition and valence state of the CdS/MoS<sub>2</sub>/Mo sheets, the X-ray photoelectron spectroscopy (XPS) analysis was performed, as shown in Fig. 3. The XPS survey spectrum shows that Cd, Mo and S elements coexisted in the system, further confirmed the coexistence of MoS<sub>2</sub> and CdS (Fig. 3a). Fig. 3b shows the high-resolution XPS spectrum of Cd 3d, which can be resolved into two peaks with the binding energy of 405.3 eV and 412.1 eV assigned to the characteristic spectra of Cd<sup>2+</sup> in CdS (Fig. S1). As shown in Fig. 3c, the XPS spectra of Mo 3d can be resolved into four peaks at around 235.4 eV, 232.5 eV, 231.6 eV and 228.5 eV, respectively. The strongest peaks at 231.6 eV and 228.5 eV can be assigned to Mo (+4) 3d<sub>3/2</sub> and Mo (+4) 3d<sub>5/2</sub>, respectively. Compared with the previous report [29], the Mo 3d peaks in the XPS spectrum of CdS/MoS<sub>2</sub>/Mo sheets and MoS<sub>2</sub>/Mo sheets (Fig. S1) shifting towards lower energy indicates that there are binding between Mo sheets and MoS<sub>2</sub>. The peaks at 235.4 eV and 232.5 eV

correspond to Mo (+6) 3d orbit, which may be due to the exposure to air [30]. However, no Mo (0) was detected due to that the Mo sheets are as core and the XPS is the surface analysis technique. Fig. 3d shows that the S 2p peak can be resolved into two components (S 2p<sub>3/2</sub> at 161.5 eV and S 2p<sub>1/2</sub> at 162.8 eV). Besides, the binding energy at 164.4 eV is due to the presence of bridging disulfides S<sub>2</sub><sup>2-</sup>, which has been reported to be related to high activity HER species [31].

The highly active photocatalytic system needs the photocatalyst with high light absorption ability and the co-catalysts with the efficient electrocatalytic property. Fig. 4a shows the UV-vis absorption spectra of CdS (spherical morphology as shown in Fig. S2a), MoS<sub>2</sub>/Mo sheets (porous sheet structure as shown in Fig. S2b) and CdS/MoS<sub>2</sub>/Mo porous sheets. For the pure CdS nanoparticles, a significant absorption edge at around 570 nm was observed, corresponding to a band gap of ~2.18 eV (Fig. S3). The MoS<sub>2</sub>/Mo sheets sample exhibits a flat plot with a high adsorption coefficient throughout the UV-vis wavelength range, which can be attributed to the intrinsic background absorption of black colored Mo sheets and MoS<sub>2</sub>. After the MoS<sub>2</sub> and CdS simultaneously grew on the Mo sheets, the absorption spectra exhibit both the absorption characteristics of CdS and MoS<sub>2</sub>/Mo sheets. Furthermore, the enhancement of absorption intensity in all the UV-vis wavelength range was also observed. This result indicates that the addition of Mo sheets and MoS<sub>2</sub> significantly enhanced the absorption wavelength range and light trapping capability of CdS.

The HER electrocatalytic activity of the pure CdS, MoS<sub>2</sub>/Mo sheets and CdS/MoS<sub>2</sub>/Mo porous sheets system was investigated

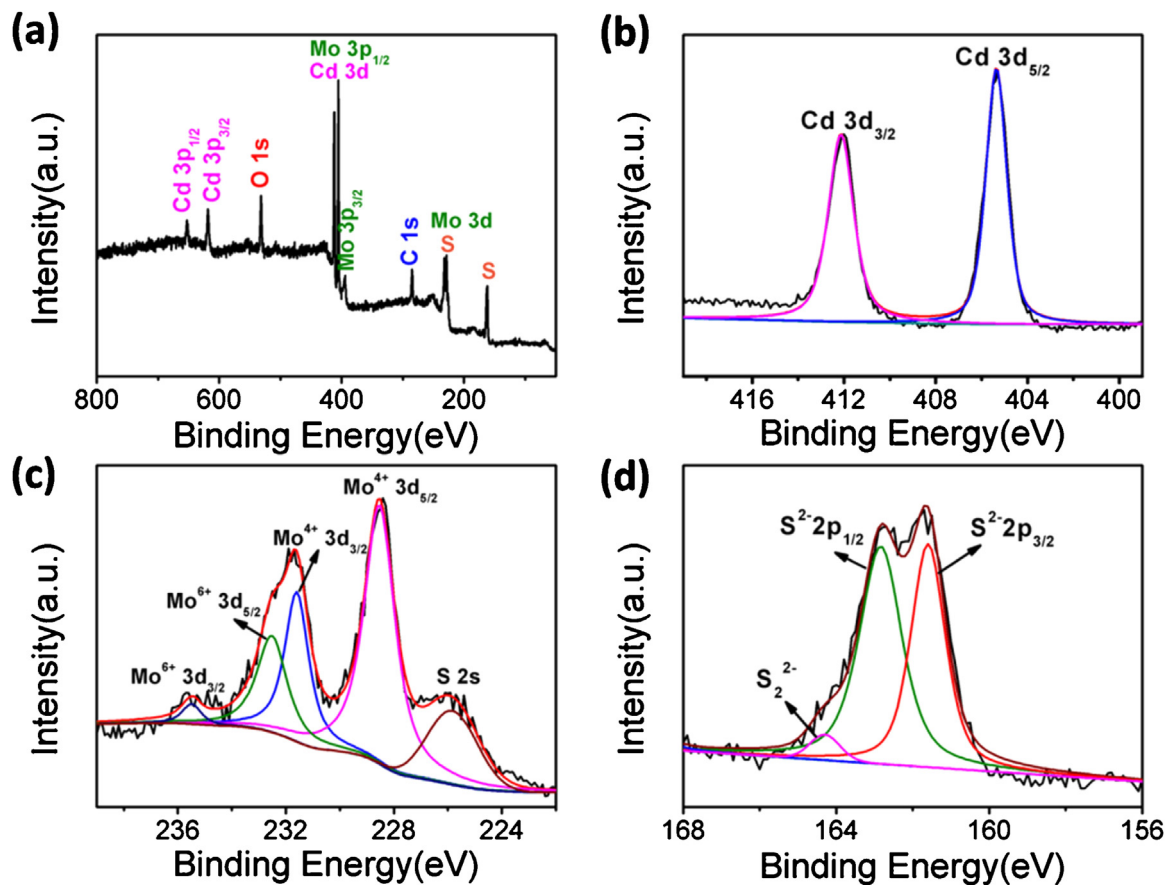


Fig. 3. XPS spectra of CdS/MoS<sub>2</sub>/Mo sheets: (a) Survey spectra, high-resolution signals of (b) Cd 3d, (c) Mo 3d and (d) S 2p.

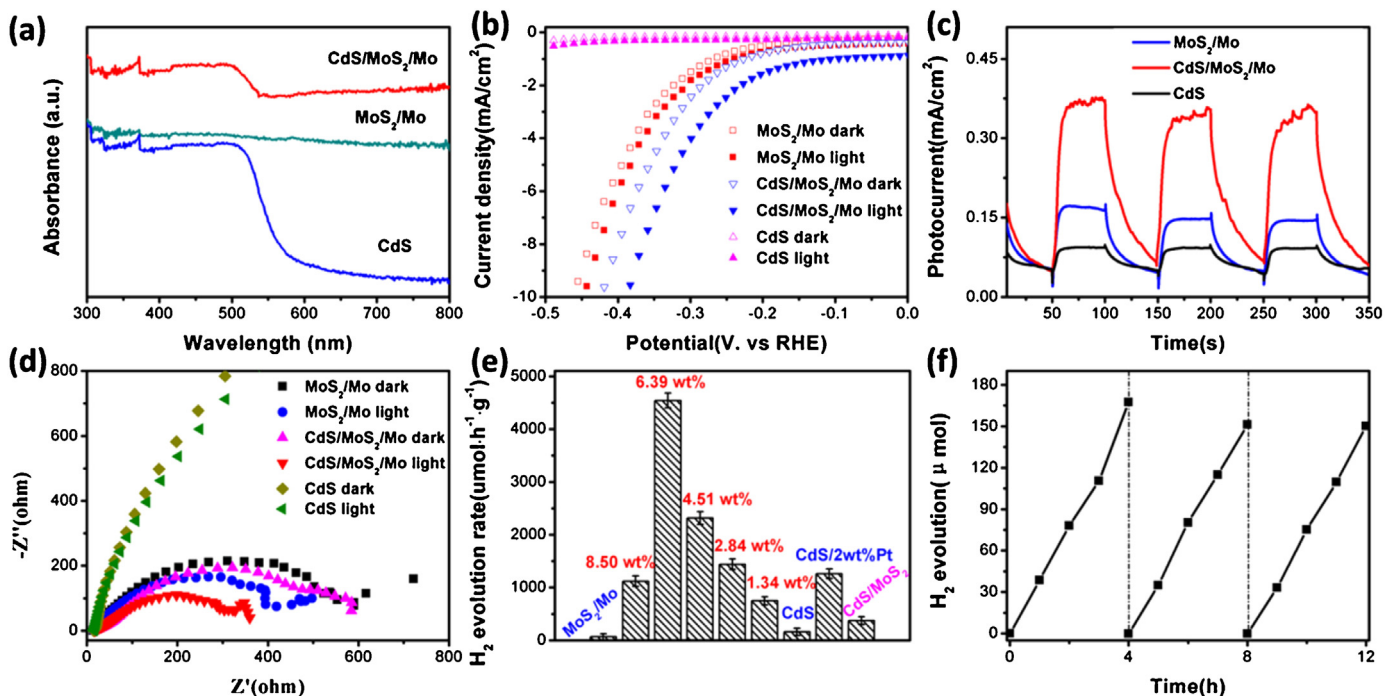
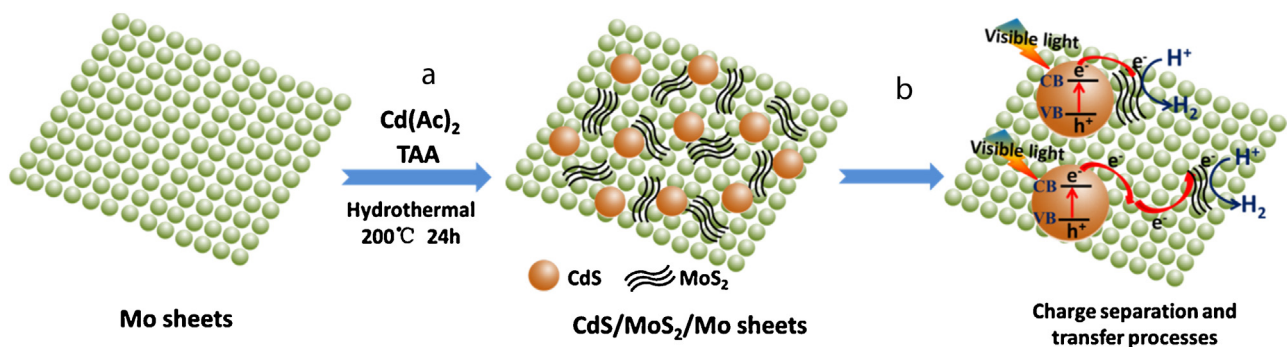


Fig. 4. Photocatalytic property of MoS<sub>2</sub>/Mo sheets, CdS/MoS<sub>2</sub>/Mo porous sheets and CdS: (a) UV-vis absorption spectra, (b) Polarization curves, (c) PEC current responses and (d) Electrochemical impedance spectroscopy Nyquist plots, (e) Photocatalytic H<sub>2</sub> evolution activity, (f) Recycling test of photocatalytic H<sub>2</sub> evolution.



**Fig. 5.** Schematic illustration of preparation of CdS/MoS<sub>2</sub>/Mo porous sheets photocatalytic system, as well as the charge separation and transfer process for enhanced photocatalytic H<sub>2</sub> evolution.

in 0.5 M H<sub>2</sub>SO<sub>4</sub> solution by employing a typical three-electrode setup under the dark and light condition, including the linear sweep voltammetry, photocurrent response, and electrochemical impedance spectroscopy. The polarization curves in Fig. 4b show that pure CdS nanoparticles exhibit the negligible HER activity. As a contrast, the CdS/MoS<sub>2</sub>/Mo porous sheets system possess high electrocatalytic activity for HER with the low overpotential of 420 mV (10 mA/cm<sup>2</sup>), which is also better than that of MoS<sub>2</sub>/Mo sheets (460 mV) possibly due to the more exposed active sites caused by the embedded CdS photocatalyst. It is more important that the enhanced photoresponse of CdS/MoS<sub>2</sub>/Mo under light irradiation can be detected due to the efficient photocatalyst of CdS. The corresponding current density of CdS/MoS<sub>2</sub>/Mo sheets at 0.35 V vs. RHE was improved about 47.1%, which is much larger than that of MoS<sub>2</sub>/Mo sheets (14.4%), indicating a highly active photocatalytic system. As shown in Fig. 4c, the CdS/MoS<sub>2</sub>/Mo porous sheets sample exhibits the highest photocurrent density compared with MoS<sub>2</sub>/Mo sheets and pure CdS, indicating the longest lifetime of photogenerated charge carriers due to the heterostructure effect of MoS<sub>2</sub>/CdS and electron bridge effect of Mo metal sheets. Fig. 4d shows the electrochemical impedance spectroscopy (EIS) Nyquist plots of these three samples under dark and light condition. As reported [32], the depressed semicircle in the high-frequency region is attributed to charge transfer resistance (R<sub>ct</sub>), which is related to the electrocatalytic kinetics and its lower value corresponds to the faster reaction rate. As shown in Fig. 4d, the CdS/MoS<sub>2</sub>/Mo porous sheets system displays the smallest R<sub>ct</sub> value among these three samples, no matter in dark or under light illumination, which is consistent with the results of polarization and photocurrent measurements. The low R<sub>s</sub> value of CdS/MoS<sub>2</sub>/Mo sheets is attributed to the good electrical conductivity from Mo sheets. In addition, the largest changed R<sub>ct</sub> value of CdS/MoS<sub>2</sub>/Mo sheets under light illumination compared with that in the dark also confirm the most efficient photocatalytic system.

Concluded with the above results, CdS as photocatalyst significantly enhances the photoresponse, and the presence of MoS<sub>2</sub> nanosheets as co-catalysts provides catalytically active sites for H<sub>2</sub> evolution and the Mo sheets as conductive supports improve the electrical conductivity. It suggests that the CdS/MoS<sub>2</sub>/Mo porous sheets should be an efficient photocatalytic H<sub>2</sub> production system. As shown in Fig. 4e, as the comparison, the very low rates of photocatalytic H<sub>2</sub> evolution for MoS<sub>2</sub>/Mo sheets and CdS nanoparticles are 67.4  $\mu\text{mol h}^{-1} \text{g}^{-1}$  and 159  $\mu\text{mol h}^{-1} \text{g}^{-1}$ , respectively. However, the CdS/MoS<sub>2</sub>/Mo sheets photocatalytic system exhibits a noticeable enhancement of photocatalytic hydrogen production activities. The optimized loading amount of MoS<sub>2</sub> in CdS/MoS<sub>2</sub>/Mo sheets was also evaluated, and the XRD pattern confirmed the composition changes (Fig. S4). With the optimal MoS<sub>2</sub> loading amount of 6.39 wt%, the highest photocatalytic activity of

CdS/MoS<sub>2</sub>/Mo sheets was obtained with the H<sub>2</sub> evolution rate as high as 4540  $\mu\text{mol h}^{-1} \text{g}^{-1}$ , which is higher than those from the MoS<sub>2</sub> loading amounts of 8.50 wt% (1120  $\mu\text{mol h}^{-1} \text{g}^{-1}$ ), 4.51 wt% (2000  $\mu\text{mol h}^{-1} \text{g}^{-1}$ ), 2.84 wt% (1350  $\mu\text{mol h}^{-1} \text{g}^{-1}$ ) and 1.34 wt% (749  $\mu\text{mol h}^{-1} \text{g}^{-1}$ ), as shown in Fig. 4e. It is because that a small loading amount of MoS<sub>2</sub> can not provide sufficient active site for proton reduction, while an excessive loading amount of MoS<sub>2</sub> may hinder the light absorption of CdS. It is more important that the optimal photocatalytic H<sub>2</sub> production rate of CdS/MoS<sub>2</sub>/Mo porous sheets is also much larger than that of CdS/2 wt% Pt (1259  $\mu\text{mol h}^{-1} \text{g}^{-1}$ ), which is an efficient catalyst for photocatalytic H<sub>2</sub> evolution [33]. The apparent quantum efficiency (QE) of these samples were also shown in Table S1 in the supporting information. It indicates that simultaneously containing co-catalysts and conductive supports is more favorable for the photocatalytic HER.

At last, to confirm the effect of Mo sheets on the photocatalytic H<sub>2</sub> evolution activity, the experiments using MoO<sub>3</sub> as Mo source was performed to synthesize CdS/MoS<sub>2</sub> without Mo sheets. As shown in Figs. S5 and S6, the XRD pattern and SEM images confirm the MoS<sub>2</sub>/CdS nanosheets. The according rate of photocatalytic H<sub>2</sub> evolution (Fig. 4e) for the MoS<sub>2</sub>/CdS (~370  $\mu\text{mol h}^{-1} \text{g}^{-1}$ ) is much lower than that activity of the CdS/MoS<sub>2</sub>/Mo porous sheets, indicating Mo sheets serve as the conductive support to improve the photogenerated electrons transfer to obtain high photocatalytic H<sub>2</sub> evolution activity. In addition, the cyclic test of CdS/MoS<sub>2</sub>/Mo sheets system was performed by using the same catalyst for photocatalytic H<sub>2</sub> evolution for prolonged irradiation of 12 h in Fig. 4f. After three recycles, there is no significant loss of activity for the catalysts, which suggests its high stability during the photocatalytic H<sub>2</sub> evolution.

In summary, the schematic illustration of the synthetic procedure for CdS/MoS<sub>2</sub>/Mo sheets and the mechanism of the improved photocatalytic activity were shown in Fig. 5. The CdS/MoS<sub>2</sub>/Mo porous sheets photocatalytic system was synthesized via a simple one-step hydrothermal method, as shown in Fig. 5a. After introducing cadmium acetate and sulfurization, CdS and MoS<sub>2</sub> nanosheets grew on the surface of Mo sheets with more effective interfaces, which were confirmed by TEM images and XPS spectra (Figs. 2 and 3). This strong chemical bonding is beneficial to photogenerated electrons transferring from CdS to MoS<sub>2</sub> co-catalyst. The mechanism of the improved photocatalytic activity of CdS/MoS<sub>2</sub>/Mo porous sheets is proposed in Fig. 5b. As shown, under the visible-light irradiation, photogenerated electrons are excited from the valence band (VB) to the conduction band (CB) of CdS photocatalyst. A portion of the photogenerated electrons can directly transfer from the surface of CdS to MoS<sub>2</sub> co-catalyst via heterostructure effect, where MoS<sub>2</sub> nanosheets act as the active sites for H<sub>2</sub> evolution. Most of the photogenerated electrons produced

from CdS rapidly transferred to Mo sheets due to the excellent electrical conductivity and Schottky effect [34], and then migrate to MoS<sub>2</sub> co-catalyst to react with the adsorbed H<sup>+</sup> to form H<sub>2</sub>. The Mo metal sheets as the electron bridge can promote the separation of electron-hole pairs and caused the longer lifetime of photogenerated charge carriers. Based on the above results and discussion, it can be concluded that the as-obtained CdS/MoS<sub>2</sub>/Mo sheets system has three principal advantages for enhanced photocatalytic H<sub>2</sub> evolution activity. Firstly, the worm-like pores and nanosheet morphology of MoS<sub>2</sub> on the surface of Mo sheets significantly improve the specific area of CdS/MoS<sub>2</sub>/Mo sheets system; Secondly, the presence of Mo sheets with good electrical conductivity facilitates fast photogenerated electrons transfer from CdS photocatalysts to MoS<sub>2</sub> co-catalysts; Lastly, the synthesized MoS<sub>2</sub> is a promising co-catalyst to provide active sites for proton reduction and inhibit charge carriers recombination.

#### 4. Conclusion

A CdS/MoS<sub>2</sub>/Mo porous sheets system simultaneously containing photocatalysts, co-catalysts, and conductive supports was prepared via a simple one-step hydrothermal method by using the Mo sheet as template and Mo source. The synergistic effect of MoS<sub>2</sub> co-catalysts and Mo sheets conductive supports contributes to the dramatically improved photocatalytic H<sub>2</sub> evolution activity of CdS photocatalyst, by means of facilitating charge carriers separation and providing active sites for proton reduction. This photocatalyst exhibits significantly enhanced activity in photocatalytic H<sub>2</sub> evolution with H<sub>2</sub> evolution rate as high as 4540 μmol h<sup>-1</sup> g<sup>-1</sup> and rough catalytic stability. This novel study provides a straightforward and effective route to produce cheap and efficient co-catalysts for large-scale water splitting.

#### Acknowledgements

This work was supported by Project of Public Interest Research and Capacity Building of Guangdong Province (2014A010106005), Guangdong Innovative and Entrepreneurial Research Team Program (2014ZT05N200) and the National Natural Science Foundation of China (51502096, 51372142).

#### Appendix A. Supplementary data

Supplementary data associated with this article can be found, in the online version, at <http://dx.doi.org/10.1016/j.apcatb.2017.04.003>.

#### References

- [1] A. Antzara, E. Heracleous, D.B. Bukur, A.A. Lemonidou, *Int. J. Greenh. Gas Control* 32 (2015) 115–128.
- [2] R.Y. Chein, Y.C. Chen, J.N. Chung, *J. Membr. Sci.* 475 (2015) 193–203.
- [3] Y. Zhao, X. Jia, G.I.N. Waterhouse, L.-Z. Wu, C.-H. Tung, D. O'Hare, T. Zhang, *Adv. Energy Mater.* 6 (2016) 1501974.
- [4] Y. Zhao, G. Chen, T. Bian, C. Zhou, G.I.N. Waterhouse, L.-Z. Wu, C.-H. Tung, L.J. Smith, D. O'Hare, T. Zhang, *Adv. Mater.* 27 (2015) 7824–7831.
- [5] L. Wei, Y. Chen, J. Zhao, Z. Li, *Beilstein J. Nanotechnol.* 4 (2013) 949–955.
- [6] J. Chen, D. Zhao, Z. Diao, M. Wang, S. Shen, *Sci. Bull.* 61 (2016) 292–301.
- [7] C.D. Giovanni, Á. Reyes-Carmona, A. Coursier, S. Nowak, J.M. Grenèche, H. Lecoq, L. Mouton, J. Rozière, D. Jones, J. Peron, M. Giraud, C. Tard, *ACS Catal.* 6 (2016) 2626–2631.
- [8] A. Fujishima, K. Honda, *Nature* 238 (1972) 37–38.
- [9] W. Zhou, Z. Yin, Y. Du, X. Huang, Z. Zeng, Z. Fan, H. Liu, J. Wang, H. Zhang, *Small* 9 (2013) 140–147.
- [10] J. Tian, Y. Leng, Z. Zhao, Y. Xia, Y. Sang, P. Hao, J. Zhan, M. Li, H. Liu, *Nano Energy* 11 (2015) 419–427.
- [11] J. Tian, Z. Zhao, A. Kumar, R.I. Boughton, H. Liu, *Chem. Soc. Rev.* 43 (2014) 6920–6937.
- [12] Y. Sang, Z. Zhao, J. Tian, P. Hao, H. Jiang, H. Liu, J.P. Claverie, *Small* 10 (2014) 3775–3782.
- [13] Y.-J. Yuan, F. Wang, B. Hu, H.-W. Lu, Z.-T. Yu, Z.-G. Zou, *Dalton Trans.* 44 (2015) 10997–11003.
- [14] Y.-P. Zhu, T.-Z. Ren, Z.-Y. Yuan, *ACS Appl. Mater. Interfaces* 7 (2015) 16850–16856.
- [15] X. Zong, H. Yan, G. Wu, G. Ma, F. Wen, L. Wang, C. Li, *J. Am. Chem. Soc.* 130 (2008) 7176–7177.
- [16] W. Zhang, Y. Wang, Z. Wang, Z. Zhong, R. Xu, *Chem. Commun.* 46 (2010) 7631–7633.
- [17] T. Bian, L. Shang, H. Yu, M.T. Perez, L.-Z. Wu, C.-H. Tung, Z. Nie, Z. Tang, T. Zhang, *Adv. Mater.* 26 (2014) 5613–5618.
- [18] J. Chen, X.-J. Wu, L. Yin, B. Li, X. Hong, Z. Fan, B. Chen, C. Xue, H. Zhang, *Angew. Chem. Int. Ed.* 54 (2015) 1210–1214.
- [19] Y.P. Xie, Z.B. Yu, G. Liu, X.L. Ma, H.-M. Cheng, *Energy Environ. Sci.* 7 (2014) 1895–1901.
- [20] Q. Li, B. Guo, J. Yu, J. Ran, B. Zhang, H. Yan, J.R. Gong, *J. Am. Chem. Soc.* 133 (2011) 10878–10884.
- [21] Z.B. Yu, Y.P. Xie, G. Liu, G.Q. Lu, X.L. Ma, H.-M. Cheng, *J. Mater. Chem. A* 1 (2013) 2773–2776.
- [22] L. Wei, Y. Chen, Y. Lin, H. Wu, R. Yuan, Z. Li, *Appl. Catal. B: Environ.* 144 (2014) 521–527.
- [23] H. Yan, J. Yang, G. Ma, G. Wu, X. Zong, Z. Lei, J. Shi, C. Li, *J. Catal.* 266 (2009) 165–168.
- [24] J. Zhang, S. Liu, H. Liang, R. Dong, X. Feng, *Adv. Mater.* 27 (2015) 7426–7431.
- [25] C. Tsai, K. Chan, J.K. Nørskov, F. Abild-Pedersen, *Surf. Sci.* 640 (2015) 133–140.
- [26] L. Shang, B. Tong, H. Yu, G.I.N. Waterhouse, C. Zhou, Y. Zhao, M. Tahir, L.-Z. Wu, C.-H. Tung, T. Zhang, *Adv. Energy Mater.* 6 (2016), n/a-n/a.
- [27] Y. Hou, A.B. Laursen, J. Zhang, G. Zhang, Y. Zhu, X. Wang, S. Dahl, I. Chorkendorff, *Angew. Chem. Int. Ed.* 52 (2013) 3621–3625.
- [28] M.-Q. Yang, C. Han, Y.-J. Xu, *J. Phys. Chem. C* 119 (2015) 27234–27246.
- [29] Y. Liu, Y.-X. Yu, W.-D. Zhang, *J. Phys. Chem. C* 117 (2013) 12949–12957.
- [30] T. Weber, J.C. Muijsers, J.H.M.C. van Wolput, C.P.J. Verhagen, J.W. Niemantsverdriet, *J. Phys. Chem.* 100 (1996) 14144–14150.
- [31] H. Vrubel, D. Merki, X. Hu, *Energy Environ. Sci.* 5 (2012) 6136–6144.
- [32] W. Zhou, J. Jia, J. Lu, L. Yang, D. Hou, G. Li, S. Chen, *Nano Energy* 28 (2016) 29–43.
- [33] J. Yang, H. Yan, X. Wang, F. Wen, Z. Wang, D. Fan, J. Shi, C. Li, *J. Catal.* 290 (2012) 151–157.
- [34] X.-H. Li, M. Antonietti, *Chem. Soc. Rev.* 42 (2013) 6593–6604.